The impact of spatial-temporal averaging on the dynamic-statistical properties of rain fields

Yang, Guangguang; Ndzi, David; Grimont, Boris; Paulson, Kevin; Filip, Misha; Al-Hassani, Abdul-Hadi

Published in:
IEEE Transactions on Antennas and Propagation

DOI:
10.1109/TAP.2019.2930137

E-pub ahead of print: 29/07/2019

Document Version
Peer reviewed version

Yang, G., Ndzi, D., Gremont, B., Paulson, K., & Filip, M. (2019). The impact of spatial-temporal averaging on the dynamic-statistical properties of rain fields. IEEE Transactions on Antennas and Propagation, 2019, [AP1610-153]. https://doi.org/10.1109/TAP.2019.2930137

The Impact of Spatial-Temporal Averaging on the Dynamic-Statistical Properties of Rain Fields

Guangguang Yang, David Ndzi, Boris Grémont, Kevin Paulson, Misha Filip

***Abstract*— Knowledge of the spatial-temporal variation of rain fields is required for the planning and optimization of wide area high frequency terrestrial and satellite communication networks. This paper presents data and a method for characterizing multi-resolutions statistical/dynamic parameters describing the spatial-temporal variation of rain fields across Europe. The data is derived from the NIMROD network of rain radars. The characterizing parameters include: (i) statistical distribution of point one-minute rainfall rates, (ii) spatial and temporal correlation function of rainfall rate and, (iii) the probability of rain/no-rain. The main contributions of this paper are the assessment of the impact of varying spatial and temporal integration lengths on these parameters, their dependencies on the integration volumes and area sizes, and the model for both temporal and spatial correlation parameters.**

***Index Terms*—rainfall rate, rain characteristics, radio-wave propagation, statistical model, fitting, modelling.**

I. INTRODUCTION

RAIN induced attenuation of microwave signals at frequencies above 10 GHz is the dominant dynamic impairment on high capacity satellite and terrestrial links [1], [2]. The characterization of rain at different spatial $(L)$and temporal (T) integration lengths is important as all the rain in the first Fresnel zone of a radio link leads to attenuation [3]-[5]. Network planners and designers of physical layer fade mitigation techniques [6], [7] require knowledge of rain characteristics at smaller space (L') and time (T') scales than are typically available from radar or rain gauge measurements. This provides impetus for the development of rain models which can be used to predict rain rates at fine scales.

Rain measurements produced by rain gauge, rain radar and satellite, each have strengths and drawbacks [8]-[11]. Numerical models can be used to address their limitations and integrate their strengths appropriately, [12], [13]. For example, Maseng and Bakken [14] proposed a stochastic-dynamic time-series model for rain attenuation field simulation which was later extended to two locations in [15]. A study in [16] shows that Maseng's model also applies to rainfall rates with the same dynamic parameters. A space-time rainfall process model that describes the behavior of the stochastic structure of rain fields was proposed by LeCam [17]. Many models have subsequently been proposed, i.e. [18]-[21] and many assume that rainfall intensity exhibits a lognormal distribution [22].

An understanding of rainfall behavior in both space and time at multi-resolutions is important for the development of rain attenuation models [4]. The study in [23] investigated rainfall variability in Italy at different time scales from $30\ mins$ to $720\ mins$ using both rain gauge and weather radar data. However, this study was limited to the spatial and temporal correlation function of rain rate at different temporal scales. Luini [5] investigated the effect of space or time integration on the spatial correlation functions of rain separately but not combined. Understanding the effect of combined space-time integration on spatial correlation is important for the development of effective fade mitigation techniques as well as the space-time rain field simulators. A study by the authors highlighted the importance of space-time averaging on rain properties [3].

This paper focuses on the comprehensive study and modeling of the key rain properties over different spatial and temporal integration lengths (ranging from $5\ km$ to $75\ km$ in space and from $15\ mins$ and $1440\ mins$ in time) to investigate how scaling affects the dynamic-statistical properties of rain fields over different regions. The main aim is to ameliorate the challenges and cost of obtaining high resolutions rainfall rate characteristics over wide areas. It proposes models that can be used to obtain rain characteristics at multiple space (λL) and time (φT) scales. This paper:

- characterizes rainfall fields over different climatic zones in Western Europe based on radar measurements. As rain is irregular in both space and time domains, its key characteristics with varying space-time scales at different locations are studied and presented; and
- proposes a new space-time statistical rain model for spatial correlation and temporal variation of rain over the whole of Western Europe. Results of higher order moments of rain fields and an empirical models of rain/no rain statistics are presented.

The rest of this paper is organized as follows; Section II reviews space-time rain model implemented in this study. Details of the experimental data used are also provided. The methodology used to vary the integration length of radar data in both space and time domains is presented in Section III. Section IV describes how to characterize the rain properties as well as the technique used to integrate the data from short to longer integration lengths. Section V presents the results of rain rate statistics, spatial and temporal correlation of rain, the probability of rain/no rain and the proposed empirical models. Conclusions are drawn in Section VI.

II. SPACE-TIME MODELLING OF RAINFALL RATE

Rainfall rate, R, in mm/h at a particular location and for a particular combination of spatial and temporal integration, is modeled as a lognormal process with mixed probability density function (pdf) [1]:

Guangguang Yang, University of Portsmouth, Anglesea Building, Anglesea Road, Portsmouth, PO1 3DJ, UK. Email: guangguang.yang@myport.ac.uk. Tel: +442392842587.

David Ndzi, University of West of Scotland, Paisley, UK. Email:david.ndzi@uws.ac.uk.

Boris Gremont, University of Portsmouth, Anglesea Building, Anglesea Road, Portsmouth, PO1 3DJ, UK. Of late.

Kevin Paulson, School of Engineering, University of Hull, Cottingham Road, Hull, HU6 7RX, UK, Tel: +44 (0) 1482 465118. Email: K.Paulson@hull.ac.uk

Misha Filip, University of Portsmouth, Anglesea Building, Anglesea Road, Portsmouth, PO1 3DJ, UK. Email:misha.filip@port.ac.uk. Tel: +4423928 42310.

$$\Lambda_R(\mu,\sigma,P_0) = \begin{cases} 1-P_0 & \text{no rain} \\ \frac{P_0}{\sqrt{2\pi}R\sigma} exp\left[-\left(\frac{lnR-\mu}{\sigma}\right)^2\right] & \text{for rain} \end{cases} \quad (1)$$

where P_0 denotes the probability of rain occurrence $(R > 0)$ and $\{\mu,\ \sigma\}$ are the lognormal parameters describing the average annual distribution of rainfall rate. The statistical parameters $\{P_0,\ \mu,\ \sigma\}$ depend on the location $\mathbf{x} = (x_1,\ x_2)$, and the spatial and temporal integration lengths. Crane [1] has shown that the spatial correlation function of rain rate depends only on the separation distance between two locations and the $2D$ spatial correlation function can be assumed to be isotropic i.e. it takes the form $c_S(x,y) \equiv E[R(\mathbf{x},\ t_1)R(\boldsymbol{y},t_1)] \equiv c_S(d)$
where $d = |\boldsymbol{x} - \boldsymbol{y}|$. The temporal correlation function between rainfall rate at the same location but separated by a duration of $\tau = |t_2 - t_1|$ can be represented by $c_T(t_1,t_2) \equiv E[R(\mathbf{x},t_1)\ R(\boldsymbol{y},t_2)] \equiv c_T(\tau)$.

The assumptions of stationarity and homogeneity greatly reduce the complexity of rain field characterization. The point statistics (including rain/no-rain) and the spatial and temporal correlation function form a basic set of "key characteristics" from which rain fields can be numerically synthesized.

In [22], Bell showed how rain fields can be synthesized numerically. However he assumed that all locations within a wide area share the same statistics. This is unrealistic for large area communication networks as rainfall rate varies from location to location, influenced by factors such as climate, topography, wind, etc. Although this problem has been solved by an approach proposed by Jeannin in [24], a detailed study of the rain characteristics is needed to understand the variability of rain, especially those at multiple space and time resolutions.

III. DATA DESCRIPTION

The rainfall rate data used in this study has been obtained from UK Metrological Office NIMROD radar system in the form of composite spatial maps spanning Western Europe, produced at a temporal interval of 15 $mins$ and integrated over square regions of dimension $5\ km \times 5\ km$. The NIMROD data is available from the British Atmospheric Data Centre (BADC), one of the Natural Environment Research Council (NERC) centers for atmospheric sciences. NIMROD data is continuously updated and BADC ensures the long-term integrity of the data. Over the UK, NIMROD also provides data on a 1 km grid acquired with a sample time resolution of 5 $mins$, but with variable spatial resolution depending on the distance to the nearest radar. NIMROD data has been validated using rain gauge data by some researchers, i.e. [25], and a range of data is used to calibrate the radars. Some differences between NIMROD and rain gauge data are expected due to spatial averaging. The NIMROD 1 km data has been shown to yield unbiased estimates of annual 0.01% exceeded rain rates [26].

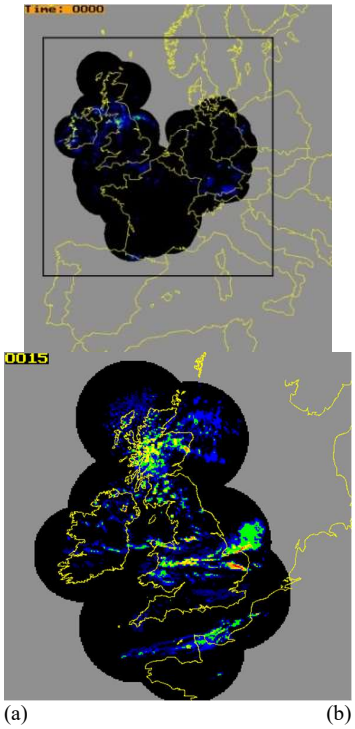

(a) (b)

Figure 1: Nimrod composite images of precipitation rates for (a) Central Western Europe with dimension of 2000 $km\ \times\ 2000\ km$, 5 km resolution and (b) British Isles with 1 km sampling.

The NIMROD network consists of 15 C-band weather radars that cover the whole British Isles. They scan at high space and time resolution over long distances. Four to five radars repeat the scan at different elevations to build 3-D scans of the area from which the best estimates of rain rates on the ground are established (details about NIMROD radar system are given in [25]). A series of composite rain field maps are then produced of rainfall rate samples on a 5 km squared Cartesian grid covering Western Europe. Each map contains $700\ \times\ 620$ data cells. However, in this study a 400×400 grid i.e. a 2000 km square region, in each radar image has been analyzed. This spans the irregular shape covered by the radars. The study area ranges from 43.1938° to 59.4306° in latitude and -9.7370° to 19.8364° in longitude. Five years of composite rain radar maps (2005 to 2009) have been analyzed in this study. The full dataset consists of more than 166000 radar maps with data availability of over 90% for each year. Fig. 1(a) shows a typical NIMROD radar scan image. The grey color is the area outside the range of the radar network where no rain data is available, and the black color represents the scanned area where data is available. A typical composite rain rate image of the UK is shown in Fig. 1(b). The validation of a model's performance requires comparisons of estimates to be made with measured data (e.g. from rain gauge or rain radar) [27]. Therefore, the 1 km grid UK data can be used to validate the results of an interpolation approach that is applied to the 5 km grid radar data for the UK.

The Nimrod system uses data collected from RHI scans at several elevations to estimate the rain rates at different altitudes, and combines these data to predict the rain rate at ground level. Due to the complex spatial-temporal processing involved, the ground rain rates are not quantized. The processing is described in [28]. The Nimrod radar provides rain-rate estimates over a large area but the resolution is not high enough for applications in radio propagation. In particular, the design and planning of the next generation satellite networks requires knowledge of rain

variation over much shorter scales i.e. a typical Fresnel zone of a few tens of meters. Because of that the NIMROD data, which is generated every 15 $mins$ on 5 km Cartesian grid, does not meet this requirement and hence the work reported in this paper.

Rain characteristics at many locations within Western Europe have been studied to reveal the impact of scaling and space-time averaging on the dynamic-statistical properties of rain fields. The latitudes and longitudes of five studied locations are listed in Table 1.

Table 1: Latitude and longitude values for five locations discussed in this paper.

Location	Glasgow	Paris	Portsmouth	Rennes	Reims
Latitude	55.8642	48.8566	50.8198	48.1173	49.2566
Longitude	-4.2518	2.3522	- 1.0879	-1.6778	4.0331

IV. CHARACTERISATION OF RAINFALL FIELDS

A. Rainfall rate

The composite map is represented on a Cartesian grid and each point contains space-time averaged rain intensity information. The average rainfall rate centered on the origin over time T and spatial area $A=L^2$ can be expressed as in [4]:

$$R(L,T) = \frac{1}{T}\int_{-T/2}^{T/2} dt \frac{1}{L^2}\int_{-L/2}^{L/2}\int_{-L/2}^{L/2} r(\boldsymbol{x},t)\, da \qquad (2)$$

where $r(\boldsymbol{x},t)$ denotes the point rainfall rate in mm/h at location $\boldsymbol{x}$ and time t on a $2D$ Cartesian grid. The interval T is the temporal integration length while L is the spatial integration length. Each NIMROD radar map consists of a Cartesian grid of such space-time averaged values. Each value is an estimate of rainfall rate at a particular instant but the algorithm for deriving the rain rate yields a value consistent with a particular integration period.

B. Key characteristics of rain

Four key rain parameters are needed to develop a space-time rain attenuation field model [3]. The principal parameter is the annual probability distribution of rain. Many studies have shown that point rainfall rate is well modeled as a log-normal random variable with a probability density function given by:

$$f(R) = \frac{1}{\sqrt{2\pi}R\sigma} exp\left(-\frac{1}{2}\left(\frac{lnR-\mu}{\sigma}\right)^2\right) \qquad (3)$$

where μ and σ are the mean and standard deviation of log rainfall rate, respectively. It is possible to transform the complementary cumulative distribution function (CCDF) to a linear relationship as described in [29]. The application of this statistical technique to different spatial and temporal integration lengths is discussed in Section V. Estimating μ and σ requires a trade-off between acquiring a large enough sample to yield significant estimates and remaining within a homogenous climate region of rain regime.

The spatial correlation function is the second important characteristic and is expressed as:

$$\rho = \frac{cov(R_1,R_2)}{\sqrt{\sigma_1\sigma_2}} \qquad (4)$$

where R_1 and R_2 are the rainfall rates (mm/hr) at two locations, 1 and 2, ρ is the cross-correlation factor between R_1 and R_2, and $cov(*)$ and σ are the covariance and standard deviation, respectively. In [3] and [22], it is assumed that the spatial correlation function of rainfall rate only depends on the separation distance i.e. the rain rate fields are spatially homogeneous, isotropic and stationary in time. These assumptions are mainly valid over small distances and times such that the shape of rain field and intermittence of rain events have no effect. Rain fronts and squalls have large linear features which are not homogeneous or isotropic over event scales. Theoretically, the correlation in space will be the same in any horizontal direction and therefore can be computed using pairs of rain rates in any orientation.

Typically, intense rain showers, which cause extreme attenuation, are of short durations. Temporal correlation quantifies how rain intensity at one particular location is correlated over different times. Temporal correlation is important as it is linked to temporal variation of fade, especially for high elevation links, which is a major input in the design of fade mitigation schemes. The development of effective route diversity or site diversity networks requires detailed knowledge of both the temporal and spatial correlation functions of rainfall rate. The temporal correlation function is defined by:

$$\rho = \frac{cov(R_{t_1},R_{t_2})}{\sqrt{\sigma_1\sigma_2}} \qquad (5)$$

where R_{t_1} and R_{t_2} are the point rainfall rates (mm/h) at two different times t_1 and t_2 but at the same location.

The last important parameter considered in this study is the probability of rain occurrence (P_0) in a geographical area, which is chosen to be of a similar size as the spot-beam of a satellite network [22]. Theoretically, P_0 (for which $R > 0$) represents equally well the expected fraction of the rainy area that one can expect for a satellite, or, the probability of rain occurrence at one point over a period of time [3]. If an unbiassed sample of rain maps is available for a homogeneous climate area, then the parameter P_0 may be estimated using:

$$P_0 \cong \frac{1}{M}\sum_1^M \frac{A_{rainy}}{A_T} \cong \frac{1}{N_T}\sum_1^{N_T} \frac{N_{rainy}}{N} \qquad (6)$$

where; A_{rainy} is the area experiencing rain within a map, A_T is the total area of the rain map of interest, M is the number of maps, N_{rainy} is the rainy sample amount at one grid point, N_T represents the total samples (including rain and no rain) at that point over a long period, and N is the total number of grid points in the area A_T.

C. Integrated rainfall data

Radar-derived space-time rainfall data typically span a larger area than rain gauge networks [27] and provides considerably denser spatial sampling. A rainfall rate map may be used to simulate the instantaneous joint fade experienced by all the links in an arbitrary microwave network [30], [31]. However, the problem lies in the reduced quality originating from the coarse sampling of measured maps as this is linked to the scan rate of the radar.

One of the key objectives of this paper is the assessment of the impact of varying spatial integration lengths and temporal integration lengths on the studied quantities. This will be useful to enhance the ability to predict the rain-induced attenuation at a range of spatial-temporal resolutions.

Let $R(x,y,t)$ be the measured rainfall rate with space resolution L and time resolution T. $R(x,y,t) = R_{ijk}$ if $iL \le x \le (i+1)L$, $jL \le y \le (j+1)L$, and $iT \le t \le (k+1)T$, otherwise $R(x,y,t) = 0$. This definition yields a three-dimensional $(3D)$ array of measured rain rate values with spatial averaging regions of size $L \times L$ and a sampling interval of T. Consider the $3D$ indicator function

$$I(x,y,t) \equiv \begin{cases} 1 & |(x,y,t)|_\infty < \frac{1}{2} \\ 0 & otherwise \end{cases} \qquad (7)$$

can be used to define how the rainfall rate changes with integration volume, where $|(x,y,t)|_\infty$ is the infinite norm. The multi-scales rainfall rate fields are defined as

$$R_\lambda(x,y,t) = \frac{1}{\lambda^3 L^2 T}\int\int\int R(x',y',t')I\left(\frac{x-x'}{\lambda L},\frac{y-y'}{\lambda L},\frac{t-t'}{\lambda T}\right)dx'dy'dt \quad (8)$$

where $R_\lambda(x,y,t)$ is the rainfall rate at position (x,y) derived from a spatial integration region of linear size $\lambda\ L$ and temporal integration time $\lambda\ T$, where $\lambda > 1$ is known as the scale parameter. More generally, the spatial and temporal regions could have different scale parameters e.g.:

$$R_\lambda(x,y,t) = \frac{1}{\lambda^2 \varphi L^2 T}\int\int\int R(x',y',t')I\left(\frac{x-x'}{\lambda L},\frac{y-y'}{\lambda L},\frac{t-t'}{\varphi T}\right)dx'dy'dt' \quad (9)$$

In particular, the integration can be divided into three categories: $2D$ spatial integration, $1D$ temporal integration, and $3D$ spatial-temporal integration. The $2D$ spatial integration only changes the integration length in the space domain at a fixed time and the $1D$ temporal integration is at a fixed location. The $3D$ integration is particularly interesting as the rain event evolves in both space and time, simultaneously. It is therefore a combination of both spatial and temporal integration.

V. EXPERIMENTAL RESULTS AND ANALYSIS

A. Statistics of rain

a) Experimental results

Generally, rain measurements are carried out at uniform time intervals. For a particular location, the annual complementary cumulative distribution function (CCDF) of point, one-minute rain intensities can be generated. In this paper, Portsmouth (UK) is taken as an example to discuss the results in detail. Fig. 2 shows the CCDF of rainfall rate conditioned on the occurrence of rain, for rainfall rate above $1\ mm/h$. It shows that the probability of a spatial-temporal volume containing rain gradually increases with the increasing integration length both in space and time domains respectively, up to around $60\ mm/h$ in space and $65\ mm/h$ in time.

Using the technique described in [29], the CCDF can be transformed to test its log-Normality. A Normal distribution leads to a straight line given by:

$$Q_{inv} = \frac{ln(R)}{\sigma} - \frac{\mu}{\sigma} \quad (10)$$

where μ and σ are the log-Normal mean and standard deviation respectively, and Q_{inv} is the inverse function of CCDF.

Fig. 3 shows the data and Least Squares (LSQ) linear regression fit to the log-Normally transformed data, for spatial integration lengths from $L = 5\ km$ to $L = 75\ km$ ($T = 15\ mins$) and temporal integration lengths from $T = 15\ mins$ to $T = 120\ mins$ ($L = 5\ km$). These results support the hypothesis that rainfall rate distributions can be well approximated by log-Normal distributions. However, note the systematic deviation for rain rates with $In(R) > 3$ for all spatial integration lengths. This is consistent with the findings in [32].

Table 2 and Table 3 list all the estimated parameter values (μ and σ) for Portsmouth for different spatial and temporal integration lengths. The value of μ gradually increases with increasing integration length meanwhile for the value of σ, the coarser the resolution the smaller it becomes. The consistency of these changes has been tested using $1\ km$ spatial grid UK NIMROD data.

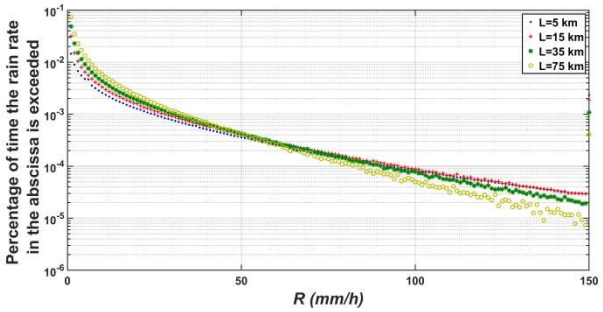

(a)

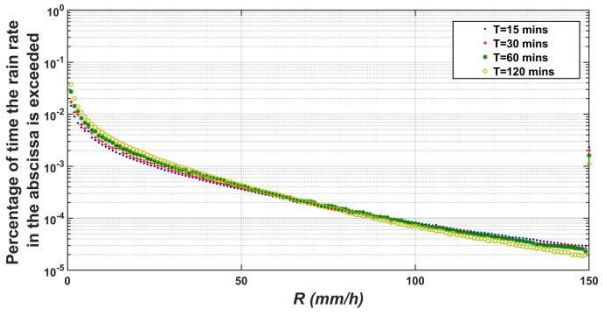

(b)

Figure 2: Averaged CCDF of five years Nimrod rainfall rate data for a range of integration lengths, (a) space domain with time interval of $\mathbf{15\ mins}$, and (b) time domain with space resolution of $\mathbf{5\ km}$.

Fig. 4 gives values of μ and σ for different map sizes, S, from $5\ km \times 5\ km$ to $530\ km \times 530\ km$, with $L = 5\ km$ and $T = 15\ mins$. It shows that both μ and σ values change significantly for small areas $S < 200\ km \times 200\ km$. These values gradually become stable and converge to constant values when the size of the map is greater than $400\ km \times 400\ km$. This happens for all spatial and temporal integration lengths (all figures are not presented in this paper). This indicates that when studying the rain field structure over a large area, the statistics of rain is independent of the map size and the integration volume is the factor that needs to be considered.

Table 2: Experimental coefficients value of log-Normal distribution parameters for different spatial integration lengths at Portsmouth ($\boldsymbol{T} = \mathbf{15\ mins}$)

$L\ (km)$	5	10	15	20	25	35
μ	−3.35	−3.21	−3.00	−2.97	−2.79	−2.67
σ	1.99	1.84	1.71	1.66	1.59	1.52
$L\ (km)$	40	45	50	55	65	75
μ	−2.60	−2.52	−2.45	−2.41	−2.33	−2.28
σ	1.48	1.49	1.43	1.39	1.31	1.22

Table 3: Experimental coefficients value of log-Normal distribution parameters for different temporal integration lengths at Portsmouth ($\boldsymbol{L} = \mathbf{5\ km}$).

$T\ (min)$	15	30	45	60	75	90	105	120
μ	−3.35	−3.16	−3.00	−2.95	−2.82	−2.78	−2.77	−2.64
σ	1.99	1.81	1.72	1.67	1.60	1.56	1.49	1.43

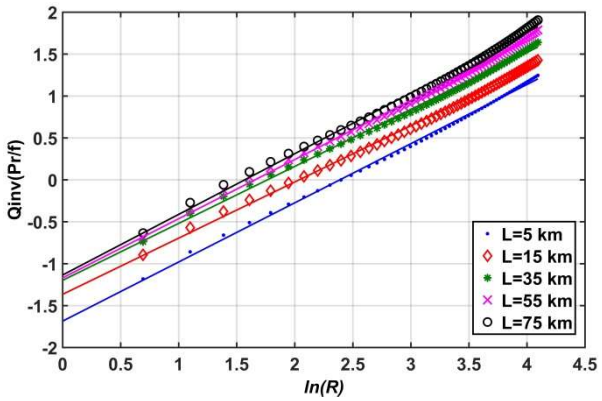

(a)

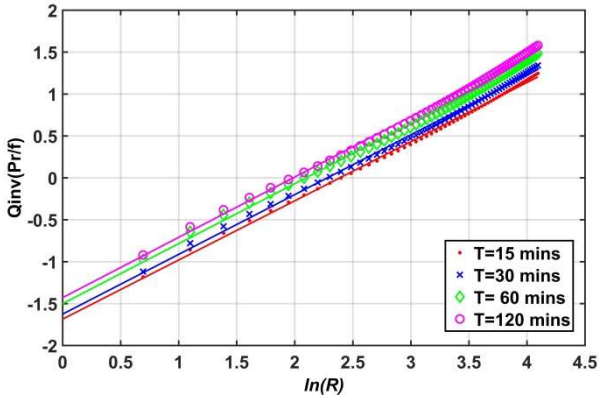

(b)

Figure 3: The test for log-Normality of rainfall rate distribution for different integration lengths, (a) space domain with time interval of $\mathbf{15}\ \boldsymbol{mins}$, and (b) time domain with space resolution of $\mathbf{5}\ \boldsymbol{km}$.

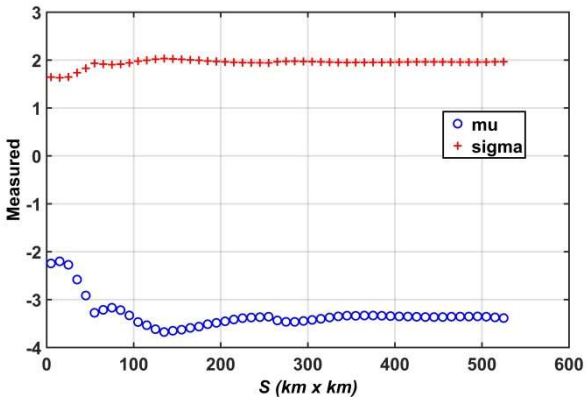

Figure 4: Experimental values of parameters of fitted lines for different map sizes $\boldsymbol{S}$ centred at Portsmouth with $\boldsymbol{L = 5\ km}$ and $\boldsymbol{T = 15\ mins}$.

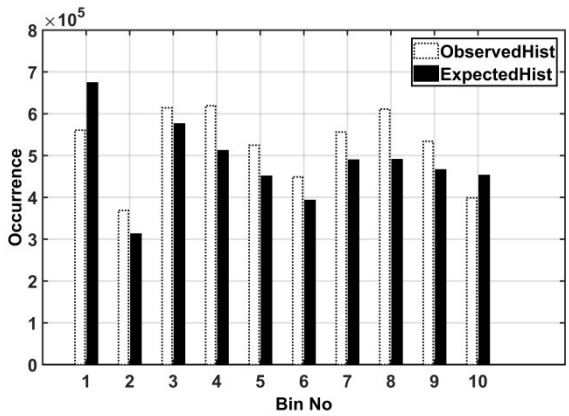

(a)

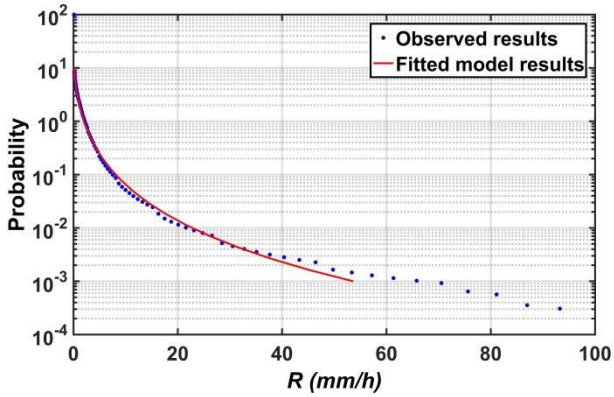

(b)

Figure 5: Comparison between observed and expected results: (a) near equal probability histograms of rainfall rate, (b) rainfall rates exceedance distribution, here $\boldsymbol{L = 5\ km}$ and $\boldsymbol{T = 15\ mins}$.

b) Validation

The Chi-squared test was applied to evaluate how well the observed trend can be used to predict rainfall at different space and time resolutions. Fig. 5(a) shows the comparison between equal-probability bin histograms of rainfall rates observed and expected ($L = 5\ km$ and $T = 15\ mins$). Fig. 5(b) show the predicted results in comparison with the measured data based on the proposed technique. Given that rainfall rates above $30\ mm/h$ is important for satellite communications, the results in Fig. 5(b) shows that the probability of rain is between 0.01% and 0.001%. The dotted line is the five year average from measured data whilst the solid line is the best fit of the model. The fitted curve appears plausible up to $35\ mm/h$, after which divergence occurs. However, it should be noted that the probability of exceedance at these higher rainfall rates are based on a small number of samples.

Fig. 6 shows the rainfall rate exceeded for 0.01% in an average year given by Rec. ITU-R P. 837-7 [33] using 1-min temporal integration length of rainfall rate. This is useful for the prediction of rain attenuation in radio communications. The rainfall rate is in the range $30\ mm/h$ to $60\ mm/h$ in Western European. In the Portsmouth area the rainfall rate exceeded for 0.01% of time is approximately $30\ mm/h$, which is larger than the $5\ km$ instantaneous 0.01% rainfall rate exceeded as shown in Fig. 5(b).

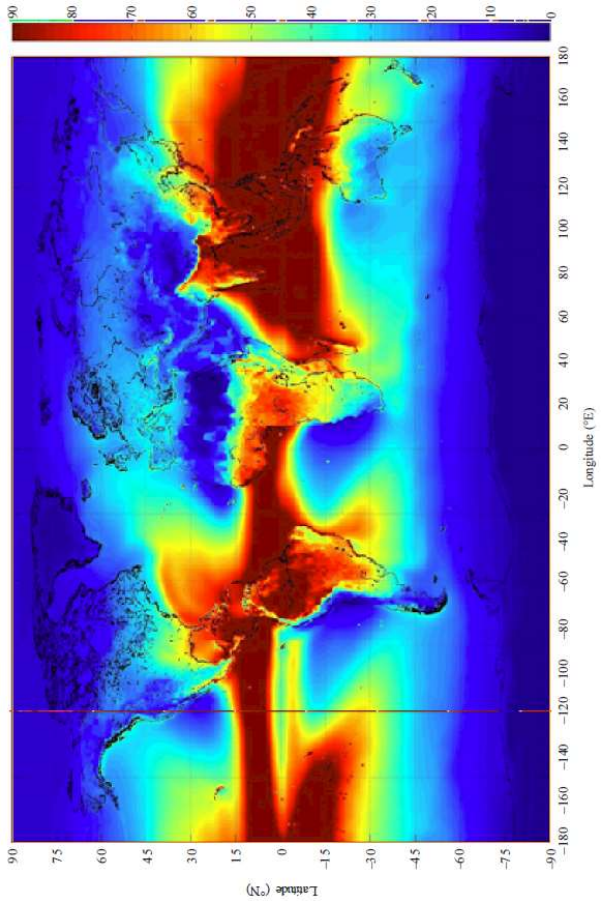

Figure 6: Rainfall rate ($\boldsymbol{mm/h}$)exceeded for $\mathbf{0.01}$% of the average year given by Rec. ITU-R P. 837-7.

The UK NIMROD data ($1\ km$ sampling in space and $5\ mins$ in time) has been integrated to form $5\ km$ by $5\ km$ grids to approximate the EU NIMROD data. Fig. 7 compares the rainfall rate exceedance distributions at Portsmouth (UK) from radar-derived EU NIMROD data and the UK data (the average of five years period). It shows that after the integration, the rainfall rate exceedance distributions generated from the different databases are in strong agreement with the plot from UK NIMROD data being slightly lower. The observed rainfall rates exceeded for 0.1%, 0.01% and 0.001% of the time from both EU and UK data at Portsmouth are $\{7.85\ mm/h, 23.9\ mm/h, 67.9\ mm/h\}$ and $\{7.6mm/h, 21.7mm/h, 66.3\ mm/h\}$, respectively.

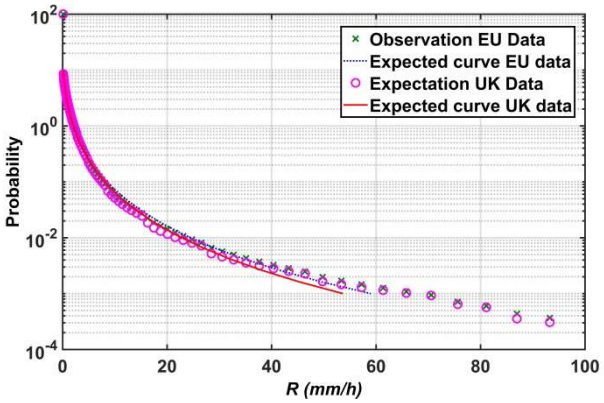

Figure 7: Comparison of rainfall rate exceedance distribution at Portsmouth using EU and UK data averaged over five years period.

B. *Correlation function of rain*

Spatial and temporal correlation functions of rainfall rate are important for rainfall field modeling and simulation [34], [35]. They vary depending on location, climate, topography, rainfall type, etc. [36]-[38]. The impact of space and time averaging on the autocorrelation function is of particular interest [3]. All these factors should be taken into account in the prediction of rain-induced attenuation.

a) Spatial correlation function of rainfall rate

The horizontal structure of rainfall fields, hence spatial correlation between two points, is important for high frequencies wireless network planning [39]. Many empirical models have been proposed and each model is derived from a study of different regions covering different continents, and for rainfall rate measurements with a range of integration volumes. The differences amongst these models indicate that the spatial structure of rainfall fields depends strongly on climate, topography, etc. Manabe and Kobayashi [40] argued that an exponential distribution is more suitable for European regions and can be adapted to other areas. Other exponential models have been proposed in [41]-[44].

This study has produced a general empirical equation that fits both the spatial and temporal correlation functions of rain rate. The generalized model is given by:

$$\rho = \frac{a}{a+x^q} \tag{14}$$

where $a > 0$ and $q > 0$ are parameters to be determined, and x can either be d (where d represents distance in km) or t (where t is the time lag in $mins$).

In this study, five years of rainfall rate data have been analyzed to estimate the spatial and temporal correlation function of rainfall rate. Fig. 8 shows the spatial correlation function of rainfall rate at Portsmouth for different spatial integration lengths ranging from $L = 5\ km$ to $L = 20\ km$. It shows that spatial correlation increases with increasing integration length due to the mixing of point covariance, with the larger covariance dominating. For example, let $C(z) = E[R(x)R(x+z)]$ be the second moment of the point rainfall rate process. For rain integrated over a line $R_D(x) = \frac{1}{2d} \times \int_{x-d}^{x+d} R(z)dz$, where d is distance, the second moment is: $R_D(x) = E[R_D(x)R_D(x+z)] = \frac{1}{(2d)^2} \times \int_{x-d}^{x+d} \int_{x+z-d}^{x+z+d} E[R(z_1) * R(z_2)]dz_1\, dz_2$.

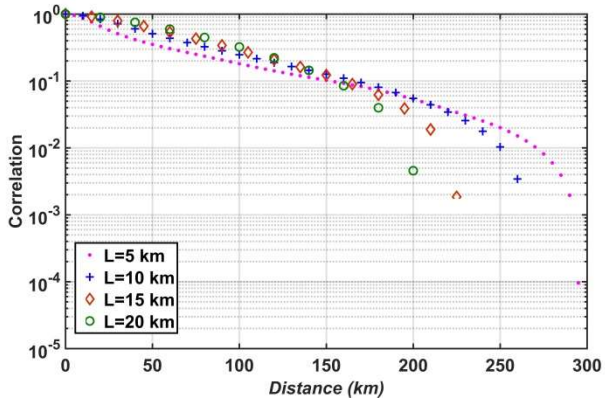

Figure 8: Spatial correlation function of rainfall rate for different spatial integration diameters at Portsmouth (here $T = 15\ mins$).

As long as $C(z)$ is decreasing and convex then $C_D(z) > C(z)$. The near linear sections of the curves (see Fig. 8) suggest exponential correlations. In particular, the $5\ km$ data suggests that there are two exponential regions: from 0 to $50\ km$ and $50\ km$ to $200\ km$. This is less obvious for larger integration length due to the effect of averaging. Fig. 9 illustrates the performance of the proposed correlation function model (Eq. (14)) against values from measured data

at 5 km in space and 15 $mins$ in time, resolutions. This shows that the correlation values can accurately be predicted using the proposed model for distances up to 150 km. The fitting has been accomplished by the minimization of the error function:

$$Error = \sum \left| Corr_{fitted} - Corr_{measured} \right| \quad (15)$$

here $Corr_{fitted}$ is the fitted correlation function and $Corr_{measured}$ is the measured value.

Note that the correlation curve falls off rapidly beyond $\mathbf{150\ km}$. There is no suitable model for distances above $\mathbf{200\ km}$, even the published models. Table 4 lists the model parameter values obtained from fitting the proposed model for different spatial integration lengths from $\mathbf{5\ km}$ to $\mathbf{20\ km}$.

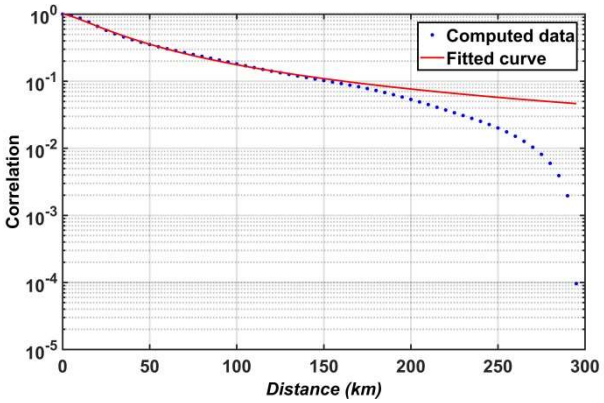

Figure 9: Example of fitted spatial correlation function of rainfall rate with $\boldsymbol{L = 5\ km}$ and $\boldsymbol{T = 15\ mins}$.

Table 4: Experimental parameter values of spatial correlation functions of rainfall rate for each spatial integration length at Portsmouth ($\boldsymbol{T = 15\ mins}$).

$L\ (km)$	5	10	15	20
a	118	494	615	884
q	1.37	1.58	1.74	1.81

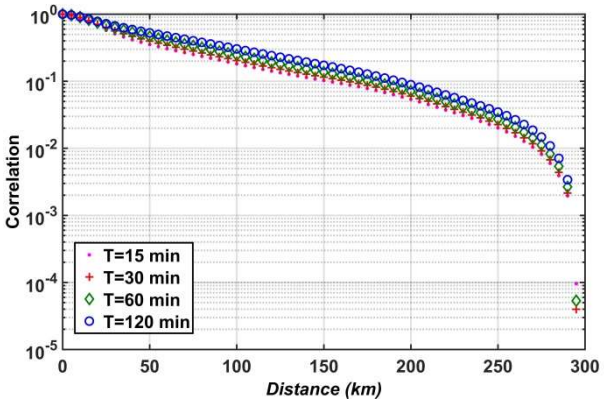

Figure 10: Spatial correlation function of rainfall rate for different temporal integration lengths at Portsmouth (here $\boldsymbol{L = 5\ km}$).

Fig. 10 shows the computed spatial correlation function of rainfall rate with different temporal averaging. The EU NIMROD data provides near-instantaneous rainfall rates at 15 $mins$ sampling intervals. Averaging n consecutive rainfall rate values for the same 5 km diameter region yields a coarse estimate of the $(n-1) \times 15\ mins$ temporal integration. It shows that temporal correlation also increases with increasing temporal integration length, similar to spatial correlation. The fitted parameter values for integration lengths from 15 $mins$ to 120 $mins$ are given in Table 6.

Table 5: Experimental parameter values of spatial correlation functions of rainfall rate for each temporal integration length at Portsmouth ($\boldsymbol{L = 5\ km}$)

$T\ (min)$	15	30	45	60	75	90	105	120
a	117	165	206	221	222	205	218	214
q	1.37	1.41	1.43	1.42	1.40	1.37	1.36	1.35

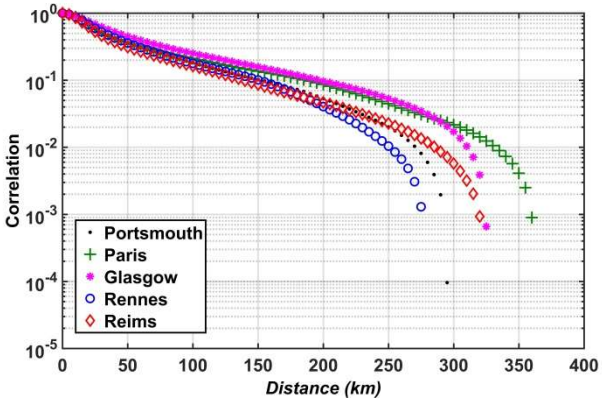

Figure 11: Comparison of spatial correlation functions of rain, for five European locations, derived from five years of radar data (here $\boldsymbol{L = 5\ km}$ and $\boldsymbol{T = 15\ mins}$).

Five locations distributed across the Western European radar scanned area were investigated to assess how spatial and temporal correlation functions of rainfall rate changes with location. Fig. 11 presents their spatial correlation functions calculated using five years of data. The spatial correlation is very close for all locations for the scales ($0 - 15\ km$), which is a typical scale for rain storms. For larger scales, the spatial correlation is more variable and differs appreciably. This is consistent with the findings of Manabe [40] who studied 8 locations in Europe. The large difference in correlation values between Paris and Rennes suggests a strong climatological or topographic dependency. It also shows that all the distributions are close to exponential over the range 50 km to 200 km. The range beyond 300 km yields negative correlation values. This could be used to optimize diversity gain when choosing locations for satellite ground stations. For all locations studied, the proposed correlation model (Eq. (14)) provides a very good fit to the calculated values. This supports results reported in [39]. In addition, the authors have relied upon the Nimrod system to produce unbiased results. Although the resolution of the data will be higher nearer radars, this should not affect the correlation. The rain fields have been assumed isotropic and so the correlations to be rotationally symmetric. A consequence of this is that correlation values are averages over a large number of data pairs in different orientations, and so errors due to the factors the reviewer raises will be averaged out. It seems more reasonable to assume that maritime and continental locations will experience a different mix of weather systems and so exhibit different correlation functions.

b) Temporal correlation function of rain rate

The temporal correlation function of rainfall rate is important for network reliability design, sufficient link power margin provision as well as adequate fade mitigation employment. Fig. 12 compares the temporal correlation functions of rainfall rate of the five European locations based on five years data. At a correlation value of 0.37 (equal to the value of $1/e$), correlation times of between 60 $mins$ and 200 $mins$ are obtained at different locations indicating a strong location dependency. Fig. 12 also shows that the

temporal correlation function of rainfall rate changes significantly with temporal integration lengths between 15 $mins$ and 120 $mins$. Similar results have been reported in [45] for sampling periods of 10 s and 1 min using data measured using a disdrometer.

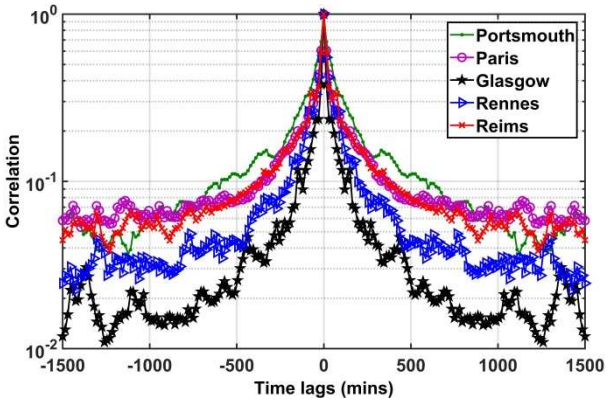

Figure 12: Temporal correlation function of rainfall rate for five European locations, here $\boldsymbol{L = 5\ km}$ and $\boldsymbol{T = 15\ mins}$.

The data and the fitted curves based on Eq. (14) for different temporal integration lengths are provided in Fig. 13. The fitted curves are in good agreement with the measured data for time lags up to 1000 $mins$. The values of the parameters of Eq. (14) for each temporal integration length are provided in Table 7.

Fig. 14 shows the short-lag temporal correlation function at Portsmouth for different spatial integration lengths ranging from $L = 5\ km$ up to $L = 75\ km$ with $T = 15\ mins$. It shows that the temporal correlation function gradually becomes smoother due to spatial averaging with increasing integration length.

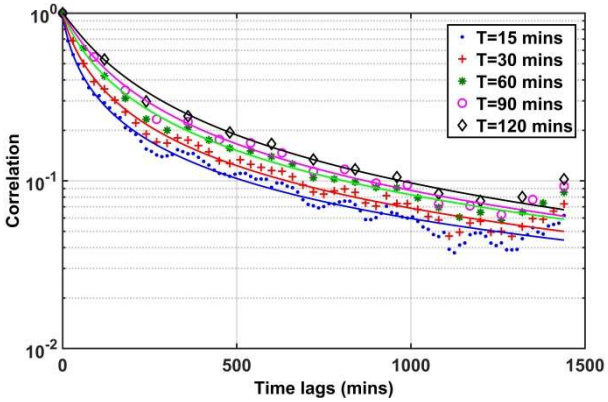

Figure 13: Fitted lines for the temporal correlation function of rainfall rate with different temporal integration lengths at Portsmouth, here $\boldsymbol{L = 5\ km}$.

Table 6: Experimental parameter values of temporal correlation function of rainfall rate for different temporal integration lengths at Portsmouth ($\boldsymbol{L = 5\ km}$).

$T\ (min)$	15	30	45	60	75	90	105	120
a	24.1	45.5	60.6	84	102	136	193	215
q	0.86	0.93	0.96	0.99	1.01	1.05	1.09	1.10

The differences between the temporal correlation between $L = 5\ km$ and $L = 75\ km$ indicate a strong integration length dependency. However, the temporal correlation falls off quickly for any spatial integration length with short time lags to below 0.37 (roughly $1/e$) at approximately 500 $mins$. The fitted parameter values of the proposed mathematical model are given in Table 8.

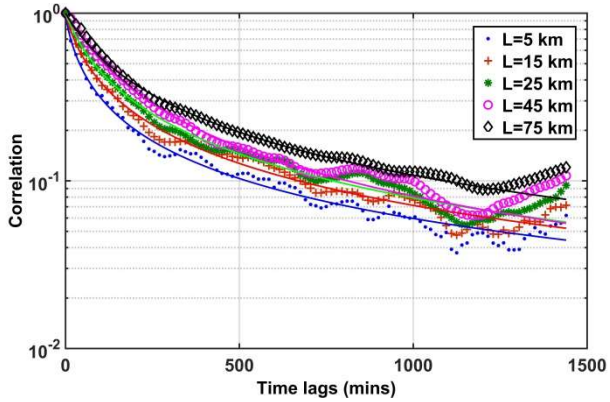

Figure 14: Temporal correlation function of rainfall rate for different spatial integration lengths at Portsmouth, here $\boldsymbol{T = 15\ mins}$.

Table 7: Fitted parameter values of temporal correlation functions of rainfall rate for each spatial integration length at Portsmouth ($\boldsymbol{T = 15\ mins}$).

L	5 km	10 km	15 km	20 km	25 km	35 km
a	24.1	24.6	44.2	59.9	74.8	87.4
q	0.86	0.87	0.92	0.96	0.98	0.99
L	40 km	45 km	50 km	55 km	65 km	75 km
a	141	176	211	266	331	383
q	1.07	1.10	1.04	1.22	1.24	1.00

Typically, the temporal correlation function of point rainfall rate is affected by advection. The variation of rainfall rate at a point is due to two processes; the evolution of the rain event and the movement of the rain event. Rain event evolution tends to be slow but dominates at time lags of 40 minutes or longer whilst the movement of rain event over a point dominates for short time lags. This variation is modeled as the movement (advection) of a fixed pattern of rain over a point using the frozen storm hypothesis [46]. It states that the statistics of rain at a point are the same as the statistics of rain along a line parallel with advection. The interpretation of this is: $R(\mathbf{x}_0, t) = R(\mathbf{x}_0 - V(t - t_0), t_0)$, where V is the advection vector, $\mathbf{x}_0$ and t_0 are an arbitrary position and time. This means that for time lags less than 40 minutes, the temporal covariance of point rainfall rate for a lag $\tau = (t - t_0)$ is the same as the spatial covariance for a spatial lag of $|V * \tau|$, assuming that the rain field is homogeneous and isotropic. The temporal correlation presented is the actual correlation experienced at a point. At short time lags it averages over the range of advection speeds experienced. For lags greater than about 40 minutes, the results are determined by a combination of the evolution of large rain events and the clustering of rain events.

c) Validation

Comparing rain model predictions with measured data is commonly used to validate model performance. The predictions of the model proposed in this paper, however, are not rainfall rates but the derived key characteristics of rain. Because of this it is necessary to compute the parameters from measured data and compare them with model predicted rain characteristics parameters to validate the model's performance.

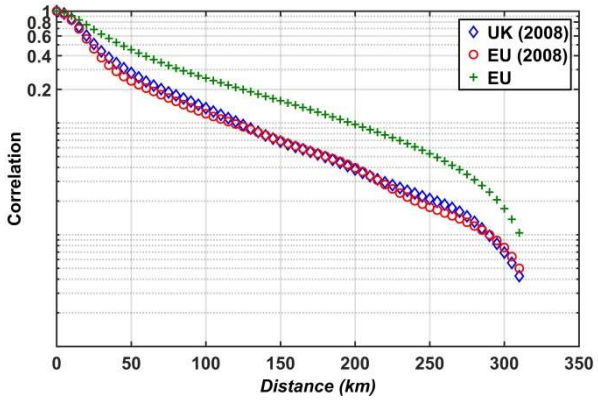

Figure 15: Comparison of spatial correlation function of rainfall rate at Portsmouth achieved from different databases ($\boldsymbol{L = 5\ km}$ and $\boldsymbol{T = 15\ mins}$).

One year of UK NIMROD data (2008) has been used to validate the model performance. The data has been up-scaled to achieve the same integration length as EU data with 5 km spatial resolution and 15 $mins$ time resolution. Fig. 15 presents the spatial correlation function of rainfall rate at Portsmouth estimated from both EU NIMROD database and UK NIMROD database. It compares UK and EU data of 2008 and a combined five years (2005 to 2009) of EU NIMROD data. The up-scaled UK 1 km grid data from 2008 yields very similar results as the EU 5 km data for the same period. This provides assurances of the validity of the approach adopted. The curve derived from combining 5 years of EU data is significantly different showing that there could have been significant year-to-year rainfall rate variations. The two near-exponential ranges, from 0 km to 50 km and between 50 km and 200 km, are present in all curves. This suggests that the same processes are present but in different proportions. This finding is in accordance with the results presented in Fig. 8 – Fig. 11.

Fig. 16 compares temporal correlation functions of rainfall rate at Portsmouth using data from EU NIMROD database and UK NIMROD database for 2008. Although there is a small difference, the results show that the proposed approach gives good estimates of data at one location.

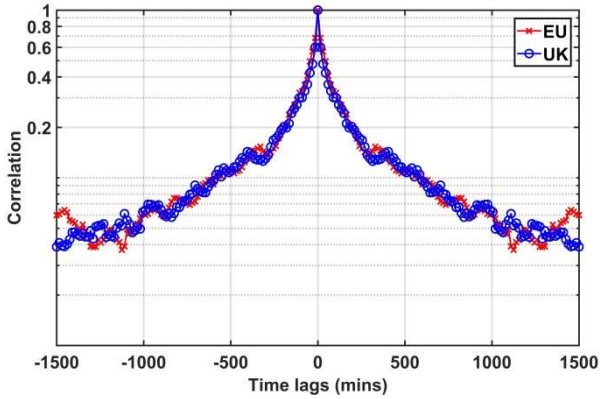

Figure 16: Comparison of temporal correlation function of rainfall rate at Portsmouth achieved from both EU NIMROD database and UK NIMROD database, for $\boldsymbol{L = 5\ km}$ and $\boldsymbol{T = 15\ mins}$.

C. Probability of rain occurrence

The probability of rain occurrence P_0 has been studied using five years of radar data. Each location has its own P_0 value and the P_0 value for any size of map can be obtained by averaging the P_0 values of all points within that map. It should be noted that the value of P_0 is poorly defined, as it is very difficult to tell whether rain is light or it is not raining at all. Its value is influenced by the way rainfall rate is measured as many instruments become unreliable at low rainfall rates. For radars, light rain could either be masked, or falsely generated, by noise within the radar equipment. In many studies, the value of P_0 is determined less by the measurements of very light rain but by the optimized fit of a rainfall rate distribution model to the full range of rainfall rates [47].

An example that reveals how the probability of rain occurrence changes with varying map sizes, S, is presented in Fig. 17. If a sufficiently long time interval is studied, the spatial variation in P_0 will exist due to orographic effects and microclimates. In this study it is assumed that the 5 years of data is sufficiently long to estimate the long-term first order statistics of rainfall rate. The P_0 is estimated through studying the proportion of 5 km cell with rainfall rates ($R > 0$) over the 5 year period. Fig. 17 shows significantly different rain probabilities between locations. This poses a significant challenge in characterizing P_0 using a generic mathematical equation that encompasses three factors; L , T and S . However, characterizing P_0 on a point-by-point basis avoids the problems introduced by averaging over inhomogeneous regions. This is the difference between the approach proposed in this paper and those reported elsewhere, where focus was on using the joint probability of rain to investigate the relationship between two locations, i.e [48]. Those researchers estimated P_0 values for un-measured location from measured ones.

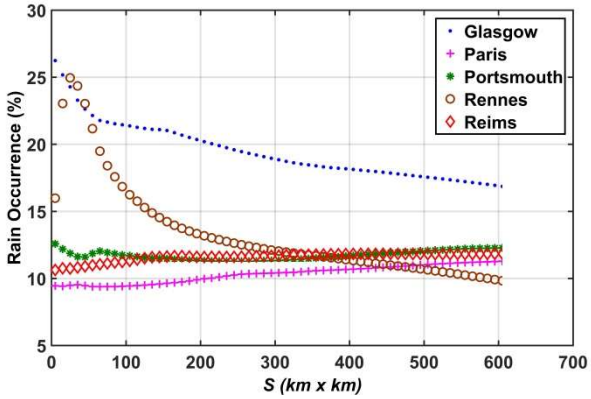

Figure 17: The variation of probability of rain occurrence for five locations changes with increasing size of map, here $\boldsymbol{L = 5\ km}$ and $\boldsymbol{T = 15\ mins}$.

According to [3], there is no easy physical way to determine P_0. In this paper P_0 has been studied from a grid point of view (with small area of $S = 5\ km \times 5\ km$, the best estimate from NIMROD radar systems for Europe) over a five years period with a range of spatial and temporal integration lengths at all locations. The results from the five studied locations are provided in this section. A mathematical equation has been proposed that gives a useful fit to the curves derived from the radar measurements:

$$P_0(x) = 100 - bexp(cx^e) \qquad (17)$$

where b , c and e are model parameters which can be determined for each location and x denotes either spatial integration length L or temporal integration length T. The equation indicates that P_0 is constrained by two factors: L and T. Hence, the values of b, c and e also exhibit variability for different spatial and temporal integration lengths.

The variation of P_0 with increasing integration length, both in space and time, together with the fitted curves are shown

in Fig. 18. P_0 is calculated using the same approach described in Section IV after integration. It shows that the value of P_0 also increases with an increase in the integration length (The same information can be found in Table 9 and Table 10). It is evident (and logical) that P_0 values will drop close to 0 when integration length approaches 0 or increase up to 100 when the integration length is long enough. Interestingly, Kundu and Siddani in [49] found the exactly the same empirical equations for the probability of rain occurrence based on raingauge data.

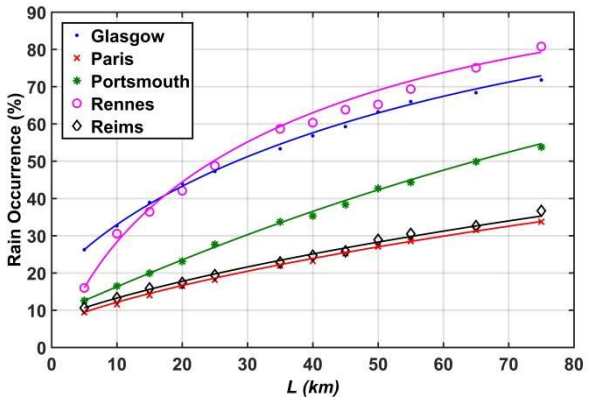

(a)

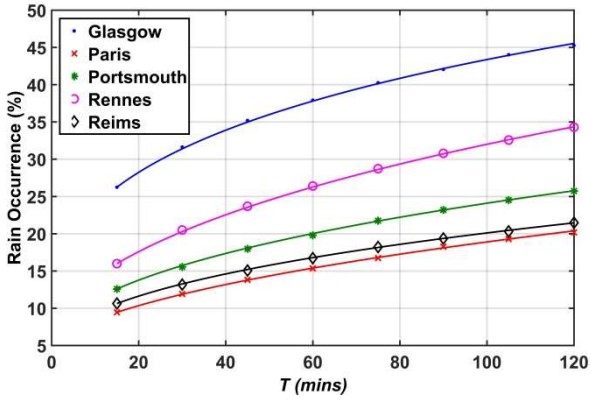

(b)

Figure 18: The probability of rain occurrence for increasing integration length in Europe: (a) $\boldsymbol{P_0}$ for different spatial integration lengths $\boldsymbol{L(km)}$, and (b) $\boldsymbol{P_0}$ for varying temporal integration lengths $\boldsymbol{T(mins)}$.

The model parameter values of Eq. (17), for each location, are presented in Table 11. The results show that the proposed P_0 expression gives good estimates throughout the whole range of integration lengths, especially in the time domain, see Fig. 18(b). This is because there are a large number of samples (five years in total) for studying P_0 in the time domain but smaller number of samples in the space domain as only one location is focused on during each processing time.

Table 8: Probability of rain at five locations with different spatial resolutions ranging from 5 km to 75 km, here $T = 15$ $mins$.

L (km)	Glasgow	Paris	Portsmouth	Rennes	Reims
5	26.2405	9.4462	12.5768	15.9804	10.6275
10	32.6411	11.5436	16.4713	30.5540	13.2886
15	38.9145	13.9786	19.9222	36.4057	15.8529
20	44.0160	16.4933	23.1190	42.0667	17.3246
25	47.2506	18.1405	27.6801	48.7526	19.4335
35	53.3291	21.9438	33.7147	58.6829	22.8025
40	56.7992	23.2056	35.2840	60.3336	24.6313
45	59.2708	25.2637	38.3525	63.8205	25.8012
50	63.2148	27.0586	42.6886	65.2125	28.8899
55	66.0124	28.5131	44.3235	69.3576	30.5064
65	68.3859	31.5219	49.8689	75.0576	32.5789
75	71.7900	33.7558	53.7848	80.7791	36.6841

Table 9: Probability of rain at five locations with different temporal resolutions ranging from 15 $mins$ to 120 $mins$, here $L = 5$ km.

$T(mins)$	Glasgow	Paris	Portsmouth	Rennes	Reims
15	26.2405	9.4462	12.5768	15.9804	10.6275
30	31.6275	11.9088	15.5298	20.4940	13.1766
45	35.1911	138133	17.9649	23.6757	15.0599
60	37.9202	15.3373	19.7803	26.4001	16.7234
75	40.2571	16.7348	21.7471	28.7198	18.2165
90	42.0518	18.2439	23.1781	30.7892	19.3508
105	44.0173	19.2713	24.5094	32.5695	20.3088
120	45.2660	20.1700	25.7226	34.2906	21.4758

Table 11: Equation 17 fitted parameters for a range of spatial and temporal integration lengths.

	Space Domain		
L (km)	b	c	e
Glasgow	83.8814	−0.0353	0.803
Paris	94.3313	−0.0113	0.798
Portsmouth	91.0541	−0.0075	1.050
Rennes	109.2417	−0.0878	0.681
Reims	92.9020	−0.0103	0.824
	Time Domain		
T $(mins)$	b	c	e
Glasgow	90.4506	−0.0623	0.438
Paris	95.6420	−0.0113	0.582
Portsmouth	95.2737	−0.0215	0.512
Rennes	93.5656	−0.0228	0.573
Reims	96.5195	−0.0213	0.474

VI. CONCLUSIONS

This paper has presented the outcome of an extensive study of five years (2005 to 2009) of rain radar data spanning the most of Western Europe. Four key characteristics of rainfall rate have been studied for a range of spatial and temporal integration lengths: (i) the annual statistical distribution, (ii) the annual spatial correlation function, (iii) the temporal correlation function, and (iv) the point probability of rain/no-rain.

It has been found that all the key characteristics of rain are strongly dependent on the spatial integration length (L) and temporal integration length (T). The results show that integration length has a significant impact on all key rain parameters owing to the high variability that rainfall intensity exhibits. This paper proposes a new model that can be used to estimate the spatial and temporal correlation of rainfall rate at different integration lengths for any location in Western Europe. The method is capable of producing estimates at spatial integration lengths from $L = 5$ km to $L = 75$ km and temporal integration lengths from $T = 15$ $mins$ to $T = 1440$ $mins$. This is critical for future simulation studies and will be highly applicable to satellite network research and planning.

The probability of rain occurrence has been shown to exhibit spatial variation over distances as short as 5 km. So far no physical equation has been found that can combine the three factors (L, T, and S) to provide good estimates of P_0. An empirical model has been proposed in this paper that can accurately estimate the P_0 value for a wide range of integration lengths; from $L = 5$ km to $L = 75$ km and between $T = 15$ $mins$ and $T = 1440$ $mins$ (one day). The

proposed model is valid when one of the spatial or temporal integration length is fixed, for a fixed map size. In short, at least two factors should be constant when utilizing the proposed model to estimate P_0 values, and the combination is either $\{L, S\}$ or $\{T, S\}$.

Finally, the results presented in this paper show that rain field structure is not constant over large areas but vary from one location to another, and this has also been partially demonstrated by some other researchers such as [5]. The statistical model proposed in this paper yields more accurate results as rain characteristics have been studied at multiple locations in a wide range of integration volumes. In particular, the proposed model significantly reduces the complexities and improves the accuracy of estimating rain characteristics and hence, radio wave attenuation, for wide area high frequency communication network planning in Western Europe.

ACKNOWLEDGEMENT

The authors thank the British Atmospheric Data Centre (BADC), which is part of the NERC National Centre for Atmospheric Science (NCAS), and the British Met Office for providing access to the NIMROD rain radar data sets. Partial support from ICT COST action IC0802, "Propagation tools and data for integrated telecommunication, Navigation and earth observation systems" is gratefully acknowledged.

REFERENCES

[1] R. K. Crane, "Electromagnetic wave propagation through rain", Wiley-Interscience, 1996.

[2] A. D. Panagopoulos and J. D. Kanellopoulos, "On the rain attenuation dynamics: spatial-temporal analysis of rainfall rate and fade duration statistics", International Journal of Satellite Communications and Networking, 21(6), 2003, pp.595-611.

[3] G. Yang, B. Gremont, D. Ndzi and D. J. Brown, "Characterization of rain fields for UK satellite networks", Ka and Broadband Communications: navigation and Earth observation conference, Oct 2011.

[4] G. Yang, "Rainfall Rate Modelling For European Satellite Networks", PhD thesis, University of Portsmouth, 2016.

[5] L. Luini and C. Capsoni, "The impact of space and time averaging on the spatial correlation of rainfall", Radio Science, 47(3), 2012.

[6] B. Gremont, M. Filip, M, P. Gallois and S. Bate, "Comparative analysis and performance of two predictive fade detection schemes for Ka-band fade countermeasures", IEEE Journal on Communications, 17(2), 1999, pp.180-192.

[7] C. Enjamio, E. Vilar, A. Redano, F. P. Fontán and D. Ndzi, "Experimental analysis of microscale rain cells and their dynamic evolution", Radio science, 40(3), 2005.

[8] D. J. Seo, W. F. Krajewski and D. S. Bowles, "Stochastic interpolation of rainfall data from rain gages and radar using cokriging: 1. Design of experiments", Water Resources Research, 26(3), 1990, pp.469-477.

[9] D. A. Hughes, "Comparison of satellite rainfall data with observations from gauging station networks", Journal of Hydrology, 327(3), 2006, pp.399-410.

[10] G. G. S. Pegram and A. N. Clothier, "High resolution space–time modelling of rainfall: the "String of Beads" model", Journal of Hydrology, 241(1), 2001, pp.26-41.

[11] K. S. Paulson, "Fractal interpolation of rain rate time series", Journal of Geophysical Research: Atmospheres, 109(D22), 2004.

[12] D. S. Wilks and R. L. Wilby, "The weather generation game: a review of stochastic weather models", Progress in Physical Geography, 23(3), 1999, pp.329-357.

[13] C. Onof, Et al, "Rainfall modelling using Poisson-cluster processes: a review of developments", Stochastic Environmental Research and Risk Assessment, 14(6), 2000, pp.384-411.

[14] T. Maseng and P. M. Bakken, "A stochastic dynamic model of rain attenuation", IEEE Transactions on Communications, 29(5), 1981, pp.660-669.

[15] B. C. Grémont and M. Filip, "Spatio-temporal rain attenuation model for application to fade mitigation techniques", Antennas and Propagation, IEEE Transactions on, 52(5), 2004, pp.1245-1256.

[16] A. Burgueno, E. Vilar and M. Puigcerver, "Spectral analysis of 49 years of rainfall rate and relation to fade dynamics", IEEE Transactions on Communications, 38(9), 1990, pp.1359-1366.

[17] L. Cam, "A stochastic description of precipitation", Proceedings of the fourth Berkeley symposium on mathematical statistics and probability 3(165-186), University of California Berkeley, Calif, 1961.

[18] J. RoldAn and D. Woolhiser, "Stochastic daily precipitation models: 1. a comparison of occurrence processes", Water resources research, 18(5), 1982, pp.1451-1460.

[19] B. C. Grémont and A. Tawfik, "Markov modelling of rain attenuation for satellite and terrestrial communications", 12th International Conference on Antennas and Propagation, 2003, pp.369-373.

[20] P. S. Cowpertwait, "A spatial–temporal point process model of rainfall for the Thames catchment, UK", Journal of Hydrology, 330(3), 2006, pp.586-595.

[21] M. Menabde, A. Seed, D. Harris and G. Austin, "Self-similar random fields and rainfall simulation", Journal of Geophysical Research: Atmospheres (1984–2012), 102(D12), 1997, pp.13509-13515.

[22] T. L. Bell, "A Space-Time Stochastic Model of Rainfall for Satellite Remote-Sensing Studies", J. Geophysical Research, Vol. 92, No D8, Aug 1987,pp. 9631-9643.

[23] M. Valeria, Et al, "Study of the rainfall dependence structure using radar and rain gauge data", International workshop Advances in statistical Hydrology, May 23-25 2010, Tormina, Italy.

[24] N. Jeannin, Et al, "A space-time channel model for simulations on continental satellite coverages: overview of the modeling and potentiality for adaptive resource management optimization", ESA Propagation Workshop, Noordwijk, The Netherlands, December 2008.

[25] B. W. Golding, "Nimrod: A system for generating automated very short range forecasts", Meteorological Applications, 5(01), 1998, 1-16.

[26] K. S. Paulson, "Trends in the incidence of rain rates associated with outages on fixed links operating above 10 GHz in the southern United Kingdom", Radio Science, 23 February 2010, https://doi.org/10.1029/2009RS004193

[27] D. A. Hughes, "Comparison of satellite rainfall data with observations from gauging station networks", Journal of Hydrology, 327(3), 2006, pp.399-410.

[28] D. L. Harrison, Driscoll S. J. and Kitchen M., (2000), Improving precipitation estimates from weather radar using quality control and correction techniques, Meteorol. Appl., 6, pp 135-144.

[29] M. Filip and E. Vilar, "Optimum utilization of the channel capacity of a satellite link in the presence of amplitude scintillations and rain attenuation", IEEE Transactions on Communications, 38(11), 1990, pp.1958-1965.

[30] K. S. Paulson and X. Zhang, "Simulation of rain fade on arbitrary microwave link networks by the downscaling and interpolation of rain radar data", Radio Science, 44(2), 2009.

[31] K. S. Paulson, L. Luini, N. Jeannin, R. Watson and B. Gremont, "simulation Review of Channel Simulators for Heterogeneous Microwave Networks", IEEE Antennas and Propagation Magazine, Vol. 55, No. 5, October 2013.

[32] B. Kedem and L. S. Chiu, "On the lognormality of rain rate", Proceedings of the National Academy of Sciences, 84(4), 1987, pp.901-905.

[33] P. Series, "Characteristics of precipitation for propagation modelling", ITU-R Recomm. P. 837-7, Geneva, 2017.

[34] K. Morita and I. Higuti, "Prediction methods for rain attenuation distributions of micro and millimetre waves", Review of the electronical communications laboratory, 24(7-8), 1976, pp.651-668.

[35] R. Berndtsson, "Temporal variability in spatial correlation of daily rainfall", Water Resource. Research, 24(9), 1988, pp.1511-1517.

[36] A. Basist, G. D. Bell and V. Meentemeyer, "Statistical relationships between topography and precipitation patterns", Journal of climate, 7(9), 1994, pp.1305-1315.

[37] H. W. Ter Maat, Et al, "Exploring the impact of land cover and topography on rainfall maxima in the Netherlands", Journal of Hydrometeorology, 14(2), 2013, pp.524-542.

[38] B. Johansson and D. Chen, "The influence of wind and topography on precipitation distribution in Sweden: Statistical analysis and modelling", International Journal of Climatology, 23(12), 2003, pp.1523-1535.

[39] H. Fukuchi, "Correlation properties of rainfall rates in the United Kingdom", Microwaves, Antennas and Propagation, IEE Proceedings H 135(2), April 1988, pp. 83-88.

[40] T. Manabe, H. Kobayashi, T. Ihara and Y. Furuhama, "Spatial correlation coefficients of rainfall intensity inferred from statistics of rainfall intensity and rain attenuation' Annales des telecommunications 41(9-10), 1986, pp.463-469.

[41] Z. ŞEN and Z. HABIB, “Monthly spatial rainfall correlation functions and interpretations for Turkey”, Hydrological sciences journal, 46(4), 2001, pp.525-535.
[42] P. V. Mandapaka, Et al, “Estimation of radar-rainfall error spatial correlation”, Advances in Water Resources, *32*(7), 2009, pp.1020-1030.
[43] K. Morita and I. Higuti, “Prediction methods for rain attenuation distributions of micro and millimetre waves”, Review of the electronical communications laboratory, 24(7-8), 1976, pp.651-668.
[44] C. Capsoni, E. Matricciani and M. Mauri, “Profile statistics of rain in slant path as measured with a radar”, Alta frequenza, 54(2), 1985, pp.50-57.
[45] G. Hendrantoro, T. Suryani and A. Mauludiyanto, “A multivariate autoregressive model of rain attenuation on multiple short radio links”, IEEE Letters on Antennas and Wireless Propagation, *5*(1), 2006, pp. 54-57.
[46] G. I. Taylor, “Statistical theory of turbulence”, Proceedings of the Royal Society of London A: Mathematical, Physical and Engineering Sciences Vol. 151, No. 873, Sep 1935, pp. 421-444.
[47] Y. Otsu, Y. Takahashi and T. Kozu, “Simultaneous occurrence probabilities of rainfall among nine locations in Japan”, Electronics Letters, 22(18), 1986, pp.937-938.
[48] F. Barbaliscia, G. Brussaard and A. Paraboni, “Characteristics of the Spatial Statistical Dependence of Rainfall Rate over Large Areas”, IEEE Transactions on Antennas and Propagation, Vol. 40 No. 1, Jan 1992.
[49] P. K. Kundu and R. K. Siddani, “Scale dependence of spatiotemporal intermittence of rain”, Water Resources Research, 47(8), 2011.